RSC Advances

PAPER

View Article Online
View Journal | View Issue

Check for updates

Cite this: *RSC Adv.*, 2024, **14**, 33471

Study of thermodynamic, transport and volumetric properties of nanofluids containing ZrO_2 nanoparticles in polypropylene glycol, polyvinyl pyrrolidone and water†

Nasrin Jebreili, Elaheh Janbezar, Mohammed Taghi Zafarani-Moattar, Hemayat Shekaari * and Behrang Golmohammadi

Zirconium dioxide (ZrO_2) nanofluids are used in cooling systems, solar energy, and heat exchangers, offering improved heat transfer and efficiency across a wide temperature range. The aim of this work was to study the influence of polypropylene glycol (PPG) and polyvinyl pyrrolidone (PVP) and aqueous solutions of them as a base fluid on stability, volumetric properties, and viscosity of nanofluids containing Zirconium oxide (ZrO_2) nanoparticles. The stability of these nanofluids has been confirmed using UV-Vis spectroscopy, and the particle size distribution of the systems using dynamic light scattering (DLS). Among these systems ZrO_2–PPG and ZrO_2–H_2O–PVP30% have appropriate stability. The density, speed of sound and viscosity of these nanofluids have been measured at T = (293.15 to 318.15) K. From these data, the excess molar volume (V_m^E) and isentropic compressibility (κ_s) have been determined. The effects of ZrO_2 nanoparticles and temperature have also been investigated on volumetric and transport properties of aqueous solutions of PPG and PVP. The (V_m^E) values were fitted to the Redlich–Kister, Ott *et al.*, and polynomial equations. Also, the isentropic compressibility (κ_s) values were correlated with the polynomial equation. The Eyring-NRTL and Eyring-mNRF models have been used for correlating of the viscosity of the nanofluids with temperature dependency. The performance of the Einstein, Brinkman, Lundgren and Batchelor models in the prediction of viscosity of the nanofluids has also been analyzed.

Received 13th August 2024
Accepted 2nd October 2024

DOI: 10.1039/d4ra05886k

rsc.li/rsc-advances

Open Access Article. Published on 22 October 2024. Downloaded on 5/3/2026 10:35:04 AM.
This article is licensed under a Creative Commons Attribution-NonCommercial 3.0 Unported Licence.

1. Introduction

Technological advancements in the field of power generation cause an increment in the creation of heat during work processes. As a result, the need to reduce the generated heat becomes more essential.[1] Nanofluids are one of the most promising cooling agent that transferring heat efficiently. These materials are suspensions of nanoparticles with the size of 1–100 nm, that possess specific characteristics such as high thermal conductivity that can make them potentially a suitable alternative to other coolers.[2] The creation of nanofluids necessitates the utilization of nanoparticles and a base fluid; these materials can be characterized by their unique properties and can offer potential applications in various fields such as heat transfer, lubrication, and advanced materials science.[3] One of the primary obstacles encountered in the utilization of nanofluids pertains to their inherent stability. The tendency of nanoparticles to agglomerate, driven by strong intermolecular forces, results in clotting and sedimentation within the channels through which nanofluids are passed. Consequently, their ability to effectively enhance thermal conductivity is hindered. As a result, increasing the stability of nanofluids can be considered a significant objective. Many researchers have applied various strategies to improve nanofluid stability; including the incorporation of surfactants, polymers, ultrasound, and mechanical agitation.[4–6] One of the cost effective methods to improve the stability of nanoparticles in a base fluid is utilization of polymers.[7]

Polymers on the other hand unlike the other applicants can be categorized as cost-effective, more accessible, that makes them a favorable and robust ingredient in the industry. One of the most important features of a polymer is that they can improve the stability of nanofluids. There are several methods to enhance the stability of nanofluids, the initial method involves the creation of an adsorbed layer, where polymers possess the ability to be adsorbed onto the surface of nanoparticles, consequently forming a protective layer. This protective layer, serves the crucial function of inhibiting direct contact between nanoparticles, thereby preventing their aggregation and accumulation within the fluid medium.[6] Furthermore, another strategy involves the generation of steric repulsion,

Department of Physical Chemistry, Faculty of Chemistry, University of Tabriz, Tabriz, 5166616471, Iran. E-mail: hemayatt@yahoo.com; Fax: +98 4133340191; Tel: +98 4133393094

† Electronic supplementary information (ESI) available. See DOI: https://doi.org/10.1039/d4ra05886k

© 2024 The Author(s). Published by the Royal Society of Chemistry

Open Access Article. Published on 22 October 2024. Downloaded on 5/3/2026 10:35:04 AM. This article is licensed under a Creative Commons Attribution-NonCommercial 3.0 Unported Licence.

where certain polymers exhibit functional groups that become ionized and charged when immersed in water. These electrically charged functional groups induce repulsive forces between nanoparticles, thereby preventing their aggregation and subsequent accumulation.[8] Moreover, polymer leads to an increase in fluid viscosity as the concentration of polymer escalates. The elevation in viscosity levels plays a pivotal role in diminishing the Brownian motion (random motion of particles immersed in fluid) exhibited by nanoparticles, consequently reducing the likelihood of their collision and subsequent aggregation within the nanofluid.[9] Lastly, polymers have the ability to induce alterations in surface energy exhibited by both nanoparticles and the base fluid. This modification in surface energy profiles exerts an influence on the intermolecular operative forces between nanoparticles and the surrounding fluid medium, consequently impacting the aggregation tendencies within the nanofluid system.[10]

PVP is a polymer that is widely utilized across various fields due to its remarkably intriguing characteristics.[11,12] Polypropylene glycol (PPG) is less toxic than polyethylene glycol (PEG) and frequently used in the pharmaceutical and cosmetic fields as solvent, carrier, humectants, lubricant, binder, base and coupling agent and also for extraction, separation, and purification of biological materials.[13,14] The utilization of (PPG) has been thoroughly examined in the presence of various fluid systems as a stabilizing agent.[15,16] Metal nanoparticles, metal oxides, carbides, nitrides or carbon nanotubes with various shapes are used in the preparation of nanofluids.[17] Among these materials, metal oxides as a nanostructure stand as a suitable candidate as they have been used in the manufacture of optical cells, electroluminescence, electrochromic windows, and chemical sensors.[18] ZrO_2 can be mentioned among these nanoparticles. ZrO_2 nanoparticles possess high mechanical properties such as high strength and flexibility, also these nanoparticles possess interesting characteristics such as heat insulation that has been widely utilized in the industrial fields.[19] Some research studies have been conducted on ZrO_2 nanoparticles. Gustaman and co-workers,[20] synthesized the ZrO_2 nanoparticles through the sol–gel method and investigated the possibility of using nanofluid containing ZrO_2 as a coolant in a nuclear reactor. They synthesized ZrO_2 nanoparticles and studied the properties of nanofluid containing ZrO_2 nanoparticles dispersed in water base fluid at different pH. The results show that the thermal conductivity of the studied nanofluid is about 4–9% higher than the base fluid. Recent studies have shown that nanofluids containing metal oxide nanoparticles dispersed in water as a fluid can increase thermal conductivity by 30–40%.[21] Moghtaderi and colleagues,[22] investigated the effect of anionic surfactants (Sodium dodecyl benzene sulfonate) on the stability and thermodynamic properties of metal oxide nanofluids containing Al_2O_3 and CuO nanoparticles.[22] ZrO_2 nanoparticles show significant physical properties, despite the excellent heat transfer properties of metal oxide nanoparticles, there are still issues to be investigated about nanofluids.[23–26] One of the basic issues in this field is the agglomeration of oxide nanoparticles in aqueous solutions, which is due to high hydrophilicity and strong Van der Waals forces.[27,28] Despite extensive measurements, the very important and practical property of nanofluids is thermal conductivity. The studies and models that have been investigated to fit thermodynamic quantities and viscosity of polymer solutions and nanofluids are often for a concentrated region, and fewer studies have been conducted in the field of thermodynamics of nanofluids in the dilute region.[29–31]

In this research, nanofluid systems including ZrO_2 nanoparticles in water, PPG and aqueous PVP as base fluids have been investigated and the thermodynamic performance and interactions in these systems have been investigated. UV-Vis spectroscopy was adopted to observe the stability of nanofluid with the passage of time. The density, speed of sound and viscosity of nanofluids including ZrO_2 nanoparticles dispersed in PPG, H_2O–PVP and H_2O have been measured up to semi-dilute concentration range at $T = (293.15, 298.15, 308.15, 318.15)$ K. For elucidating the interactions occurring in biphasic heterogeneous colloids, the excess molar volume (V_m^E) and isentropic compressibility (κ_s) which are convenient for this aim determined.[32] The V_m^E values were correlated with the Redlich–Kister,[33] Ott *et al.*[34] and polynomial equations. The κ_s values were fitted with the polynomial equation. The Eyring-NRTL[35] and Eyring-mNRF[36] models have successfully been used to correlate the viscosity reported data. Additionally, the Einstein, Brinkman, Lundgren, and Batchelor models was employed to predict the viscosity data.

2. Experimentation

2.1. Chemicals

The utilized chemicals in this work were ZrO_2, PPG and PVP. The specification about the utilized chemicals are as follows:

The ZrO_2 nanoparticles with an average diameter of 20 nm was purchased from Nanostructured & Amorphous Materials Inc., USA, polyvinylpyrrolidone (PVP) and polypropylene glycol (PPG) from Merck. The related approximate molar mass for ZrO_2 was 123.218 g mol^{-1}, for PPG was 400 and for PVP was 50 000. The utilized materials purity were >99% according to the supplier. Also, the related CAS. no. for ZrO_2 was 1314-23-4, 9003-39-8 for PVP and 25322-69-4 for PPG. The utilized water in this study for preparation of the nanofluids was double distilled deionized with conductance about 1 μS cm^{-1}.

2.2. Preparation of the nanofluids

Zirconium oxide (ZrO_2) nanoparticles were dispersed in various base fluids, including polypropylene glycol (PPG), water, and binary mixtures of water–PPG and water–polyvinylpyrrolidone (PVP) with different mass fractions of polymers. The mole fractions of the base fluids has been provided in Tables S1 and S2.† To prepare these mixtures, an analytical balance (AND, GR-202, Japan) with a precision of $\pm 1 \times 10^{-4}$ g was employed. The resulting mixtures were subjected to ultrasonic treatment for one hour using an ultrasonic bath (Grant, England) followed by 30 minutes of exposure to an ultrasonic probe device (UP400S, 400 watts, 24 kHz).

© 2024 The Author(s). Published by the Royal Society of Chemistry

Open Access Article. Published on 22 October 2024. Downloaded on 5/3/2026 10:35:04 AM.
This article is licensed under a Creative Commons Attribution-NonCommercial 3.0 Unported Licence.

2.3. Instruments and process

The whole measurements are illustrated in Fig. 1 to show the flow of the work to assess the stability of the nanofluids. The details of the measurements are described in the continuation.

2.3.1. UV-Vis and dynamic light scattering studies (DLS). The UV-Vis spectra were measured with a spectrophotometer and (Analytic Jena, SPECORD-250, Germany) in the wavelength range from 200 to 600 nm. Particle size distribution and zeta potential are measured by a DLS device (DLS, Nanotrac wave model) for the studied system in terms of stability to obtain the nanoparticle size inside the nanofluid systems.

2.3.2. Density and speed of sound measurements. Density and speed of sound for the stable nanofluid system are measured at T = (293.15 to 318.15) K by a densimeter (Anton Paar, DSA 5000, Austria). This densimeter measures the density and speed of sound with a precision of 3×10^{-6} g cm^{-3} and 0.1 m s^{-1}. The instrument was automatically thermostabilized within ±0.001 K (with a built-in Peltier temperature controller).

2.3.3. Viscosity. The viscosity of the stable nanofluid was measured by capillary viscometer, the dangling Ubbelohde-type viscometer (Julabo, MD-18V, Germany). In these viscometers, the temperature was controlled with an accuracy of 0.01 K. The passage of the time for nanofluid through the capillary tube was measured by a stopwatch. The precision of the used stopwatch was 0.01 s.

$$\eta = K \cdot d \cdot t - \frac{N \cdot d}{t^2} \quad (1)$$

$$\eta = K \cdot d \cdot (t - \theta) \quad (2)$$

In these equations: t sample passage time through the capillary tube, N and K are viscometer constants, d is nanofluid density and θ is correction factor. In these research work θ was 1.

3. Result and discussion

3.1. Stability studies

The stability of nanofluids was investigated by UV-Vis spectroscopy. First, the nanoparticles of ZrO_2 have been dispersed in PPG, water and aqueous solutions of PPG–H_2O, PVP–H_2O as base fluids. The prepared nanofluids were stirred for one hour by a magnetic stirrer, then they were respectively placed in an ultrasonic bath for 24 h, and after 24 h in an ultrasonic bath with a probe for 30 min. UV-Vis absorption spectroscopy for ZrO_2–PPG, ZrO_2–H_2O and different ratios of ZrO_2–PPG–H_2O nanofluids at ZrO_2 mole fraction of 0.00038 are shown in Fig. 2.

The UV-Vis analysis demonstrates the maximum absorption wavelength of ZrO_2–PPG is 306 nm, ZrO_2–PPG–H_2O (4 : 1) is 333 nm, ZrO_2–PPG–H_2O (3 : 1) is 309 nm and ZrO_2–H_2O have two sharp peaks in the region of 201 and 295 nm. Therefore, to check the stability of the prepared nanofluids, after sonication, their UV-Vis spectra were recorded over the time.[37] These spectra over the time for ZrO_2–PPG, ZrO_2–H_2O and different ratios of ZrO_2–PPG–H_2O nanofluids are shown in Fig. 3. As depicted in Fig. 3, the ZrO_2–PPG system has a stability about one month, and with the time elaps, the nanoparticles were sedimented.

The ZrO_2–PPG system is stable for about one month and as the times elapses, the nanoparticles begin to precipitate from the solution. The ZrO_2–H_2O system is stable for 24 h and after 24 h the intensity of absorption decreases and the sample is unstable due to the formation of clusters of ZrO_2 nanoparticles. It can be seen in Fig. 3(c) and (d) that by adding water to the ZrO_2–PPG mixture, the samples face a sharp decrease in absorption and are

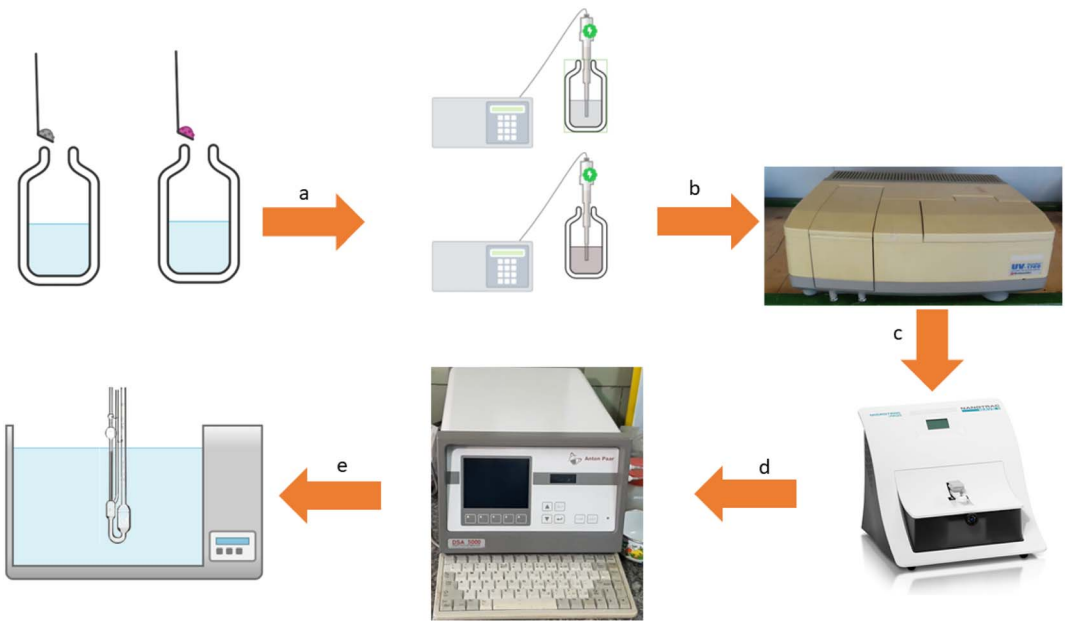

Fig. 1 The measurements diagram including preparation of mixtures and sonication (a), UV-Vis spectrophotometry (b), dynamic light scattering (c), density and speed of sound measurements (d), and viscosity measurement (e).

Open Access Article. Published on 22 October 2024. Downloaded on 5/3/2026 10:35:04 AM.
This article is licensed under a Creative Commons Attribution-NonCommercial 3.0 Unported Licence.

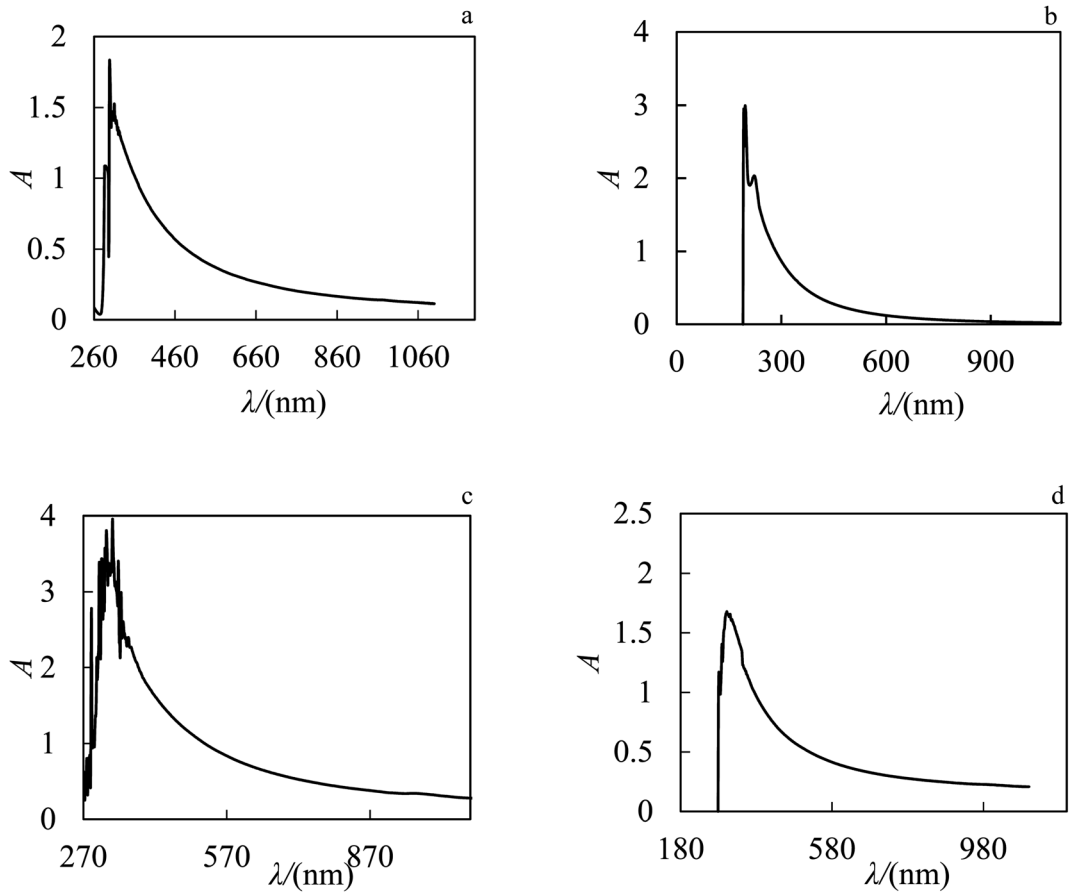

Fig. 2 UV-Vis absorption spectrum of nanofluids after ultrasonic bath (a) ZrO_2–PPG, (b) ZrO_2–H_2O, (c) ZrO_2–PPG–H_2O with ratio (4 : 1) and (d) ZrO_2–PPG–H_2O with ratio (3 : 1) of PPG–H_2O base fluid in molar fraction of ZrO_2 equal to 0.00038.

completely unstable, it can be concluded that the interactions between water molecules and PPG are more than the interaction between PPG and ZrO_2 nanoparticles, and as a result, the percentage of water compared to PPG increases, the maximum absorption decreases and ZrO_2 nanoparticles are deposited.[38–40] Among the investigated systems, the ZrO_2–PPG nanofluid exhibited satisfactory stability, as evidenced by both its intrinsic properties and thermodynamic analysis. Consequently, further thermodynamic studies can be conducted on this specific nanofluid. Fig. 4 presents the absorption–time profiles for the ZrO_2–PPG and ZrO_2–PPG–H_2O nanofluids.[38–40]

According to the results reported in the studies by Zafarani and his colleagues, the research conducted on the ZnO–PPG nanofluid system, the studied nanofluid has stability for 7 days and then with the time elaps nanoparticles start to sediment.[41] These results indicates that the ability of PPG in spreading ZrO_2 nanoparticles can be justified by the fact that with the presence of an additional oxygen in ZrO_2, more hydrogen bonds are formed with polymer molecules and the stability of the system increases. In this research, due to the instability of the ZrO_2–PPG–H_2O system, we must look for factors that increase the stability of these nanoparticles without having side effects. For this reason, PVP was used as a stabilizing agent and surfactant. In this research, in order to achieve a suitable system in terms of stability, different proportions of PVP–H_2O were prepared and ZrO_2 nanoparticles were dispersed in them. The prepared nanofluids were placed in an ultrasonic bath for 24 h and their stability over time was checked by UV-Vis and the results are shown in Fig. 5.

It is evident from Fig. 5, the absorption peak in the presence of PVP has become sharper and the maximum absorption has increased towards longer wavelengths, which indicates the larger particles, which can be attributed to the effect of PVP as a surfactant. The properties of the solvent in spectroscopy have an effect on the absorbed wavelength of the material. Therefore, the choice of solvent is important, it may be that hydrogen bonds produced by polar solvents with the ground state of polar molecules are easier than creating bonds with their excited states, as a result, the energy of electron transfers in these molecules will increase and the transfers will be towards the shorter wavelength. On the other hand, in some cases, the excited states may form stronger hydrogen bonds than the ground state, thus shifting the absorption to longer wavelengths because the electron energy decreases. By comparing the UV-Vis of ZrO_2–H_2O with ZrO_2–PVP–H_2O, it can be concluded that the systems become more stable in the presence of PVP. The interaction of PVP with ZrO_2 in the ZrO_2–H_2O system causes the stabilization of the excited state, in the 1 : 3 ratio of PVP : H_2O, the stability is higher than the other ratios. PVP is a polymer with long chains and hollow spaces, nanoparticles can enter these empty spaces due to their small size, and water

© 2024 The Author(s). Published by the Royal Society of Chemistry

Open Access Article. Published on 22 October 2024. Downloaded on 5/3/2026 10:35:04 AM.
This article is licensed under a Creative Commons Attribution-NonCommercial 3.0 Unported Licence.

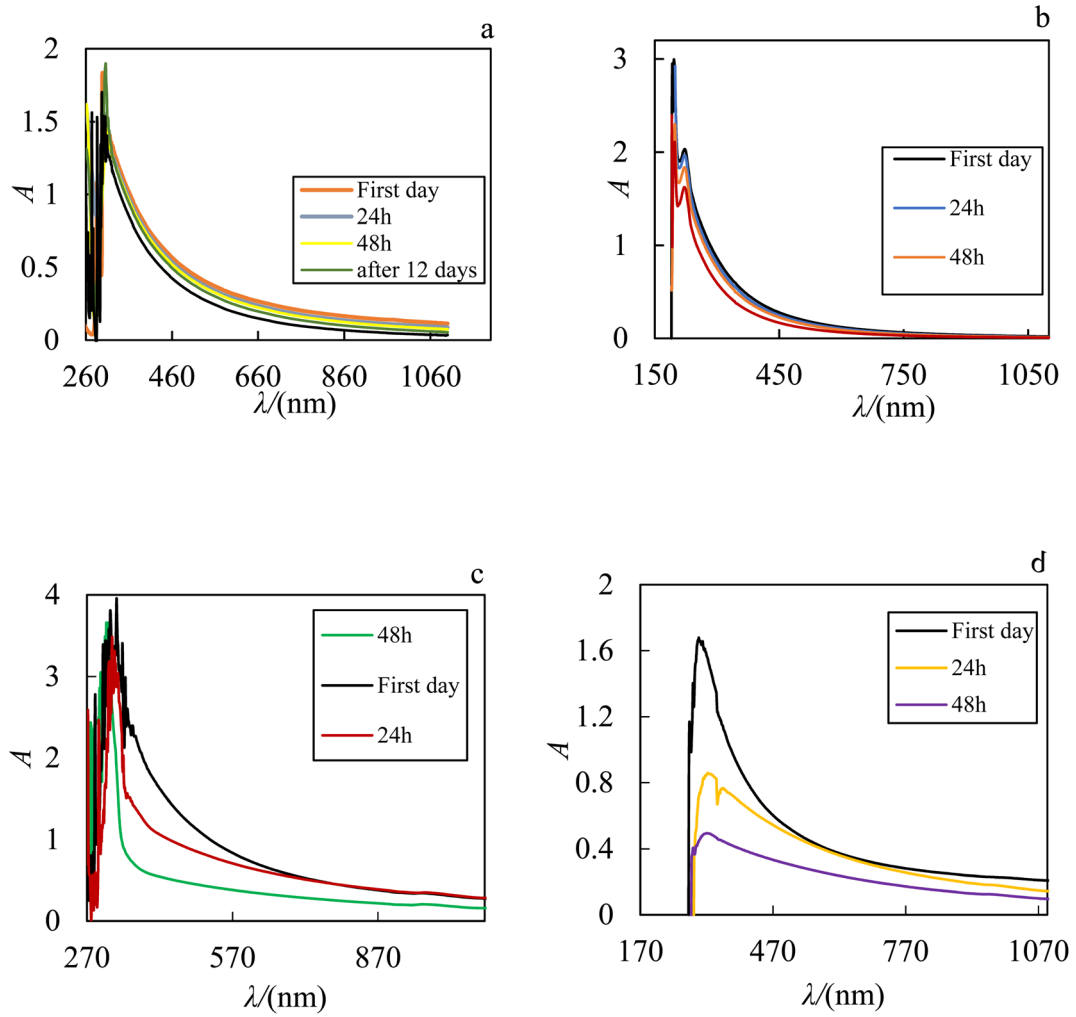

Fig. 3 UV-Vis absorption spectrum of (a) ZrO_2–PPG, (b) ZrO_2–H_2O, (c) ZrO_2–PPG–H_2O with ratio (4 : 1) and (d) ZrO_2–PPG–H_2O with ratio (3 : 1) of PPG–H_2O base fluid in molar fraction of ZrO_2 equal to 0.00038.

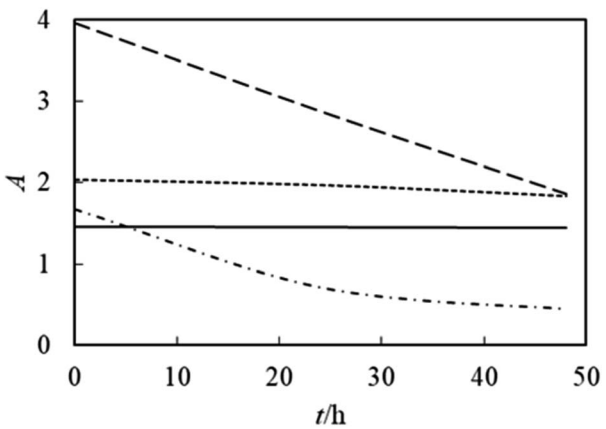

Fig. 4 UV-Vis absorption spectrum in terms of time for nanofluid ZrO_2–PPG (—), ZrO_2–H_2O (…), ZrO_2–PPG–H_2O (4 : 1) (——), ZrO_2–PPG–H_2O (3 : 1) (-.-.-.) in the molar fraction of ZrO_2 equal to 0.00038.

molecules can create strong hydrogen bonds with the polymer, and because of these strong bonds in this system, nanoparticles are more stable.

The analysis of the resulting spectra in Fig. 5 shows that by increasing the viscosity of the base fluid in the consequence of addition of polymer, the dispersion of nanoparticles improves. The UV-Vis of different ratios of ZrO_2–H_2O–PVP indicates that area under the curve in the proportions of 2%, 5%, 10% and 20% of PVP is stable for about 3 days and then decreases with the time elaps which shows the sedimentation of nanoparticles. The area under the peak decreases slowly with the increase in the amount of PVP. In the recorded UV-Vis spectrum with a ratio of 30% PVP, there is no noticeable change in the system for 5 days, and after this period of time, the amount of reduction in the area under the peak (the amount of deposition of nanoparticles) is very slow. According to these observations, the ZrO_2–H_2O–PVP system with a ratio of 30% PVP is more stable than other systems and can be introduced as an ideal fluid for ZrO_2 nanoparticles.

3.2. Particle size distribution and zeta potential

After checking the stability of the studied nanofluid systems, the particle size distribution for the stable nanofluid system containing ZrO_2 nanoparticles dispersed in PPG has been

© 2024 The Author(s). Published by the Royal Society of Chemistry

Open Access Article. Published on 22 October 2024. Downloaded on 5/3/2026 10:35:04 AM.
This article is licensed under a Creative Commons Attribution-NonCommercial 3.0 Unported Licence.

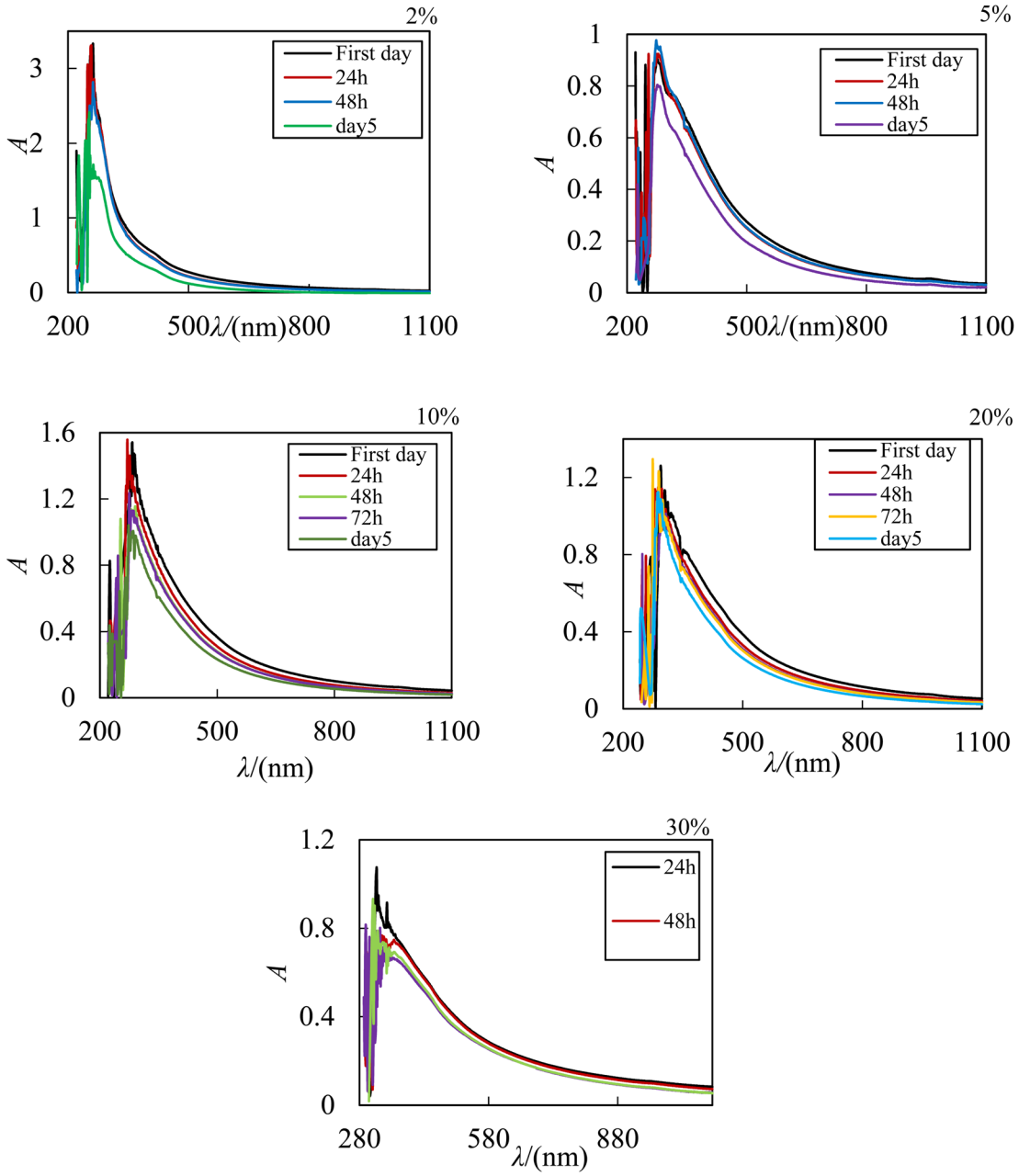

Fig. 5 UV-Vis absorption spectrum of ZrO_2–H_2O–PVP nanofluids with different ratios of PVP in ZrO_2 mole fraction equal to 0.00038.

measured by DLS. The average particle size was 163.7 nm, according to the obtained results, the average size of the nanoparticles in the fluid were larger than the initial size of the nanoparticles. In Yu and collogues studies, increasing in the size of nanoparticles was attributed to the aggregation of nanoparticles.[42] The large size of ZrO_2 nanoparticles in the fluid can be caused by the presence of long polymer chains and the particles being surrounded by polymer chains. Of course, the particles can be placed in the spaces created by the polymer, which is called the polymer compaction effect, and even this phenomenon can be considered as an effective factor in the stability of nanofluids. In a study conducted on the ZrO_2–H_2O system, it was observed that the size of the nanoparticles in the nanofluid is about 200 nm, which is more than the initial size of the nanoparticles, which was 60 nm,[43] the large size of nanoparticles in water is related to the clumping of ZrO_2 nanoparticles in water.

The zeta potential for the stable nanofluid containing ZrO_2 nanoparticles dispersed in PPG was measured and the value of +68 mV was obtained. In the study conducted on the ZrO_2–H_2O system, zeta potential for this nanofluid was +45 in acidic conditions and −41 in alkaline conditions.[44] The results reported for the zeta potential of the system, according to the studies conducted and the results obtained in the literature, systems with a zeta potential greater than +30 and less than −30 have stability.[45] Therefore, according to the size of the zeta

© 2024 The Author(s). Published by the Royal Society of Chemistry

Open Access Article. Published on 22 October 2024. Downloaded on 5/3/2026 10:35:04 AM. This article is licensed under a Creative Commons Attribution-NonCommercial 3.0 Unported Licence.

potential, it can be concluded that PPG is a suitable fluid for spreading ZrO_2 nanoparticles. These observations confirms the results of UV-Vis spectroscopy.

3.3. Density and speed of sound

In this research, ZrO_2 nanoparticles were dispersed in PPG, H_2O, PPG–H_2O and PVP–H_2O base fluids by applying ultrasonic waves. The experimental density, speed of sound and viscosity data for ZrO_2 in PPG, aqueous solution of PVP and ZrO_2 in water are collected in Table 1.

According to the results of UV-Vis spectroscopy, due to the instability of nanofluids containing ZrO_2 nanoparticles dispersed in PPG-H_2O base fluids, thermodynamic studies only on PPG and PVP–H_2O fluids were done. To compare the studied systems, density and speed of sound were measured for the H_2O–ZrO_2 system. In order to understand the interactions inside the nanofluid, the excess molar volume (V_m^E) and isentropic compressibility (κ_s) were calculated using the experimental data of density and sound speed through the following equations:[46,47]

$$V_m^E = \sum_{I=1}^{n} x_1 M_1 \left[\frac{1}{d} - \frac{1}{d_1}\right] \quad (3)$$

$$\kappa_s = \frac{1}{du^2} \quad (4)$$

where x is the mole fraction, M is the molar mass, subscripts 1, 2 and 3 stand for ZrO_2 nanoparticles, polymer and water, respectively, while, density of the ZrO_2 nanoparticles the value of 5.98 kg m^{-3} was taken from the literature.[48] Since the concentration of the investigated mixtures is dilute, the V_m^E calculated at different temperatures are not very sensitive to this value. Accordingly, the value of 5.98 kg m^{-3} at the four investigated temperatures was used. The calculated values of V_m^E and κ_s are also reported in Table 1. It can be seen that, in all cases, the density decreased with increasing temperature, whereas the loading of nanoparticles implied higher density values, as expected.

The temperature dependency of V_m^E and κ_s for ZrO_2–PPG, ZrO_2–H_2O–PVP and ZrO_2–H_2O systems are shown in Fig. 6. Density, viscosity and speed of sound for ZrO_2–PPG and ZrO_2–H_2O–PVP nanofluid systems have been measured at different temperatures by capillary viscometer and densimeter device, the results are reported in Table 1.

As is evident from Table 1 and Fig. 6, V_m^E values are negative for ZrO_2–PPG within the dilute concentration range and become more negative with increasing concentration. The effect of temperature on the V_m^E of ZrO_2–PPG is not noticeable, however, with increasing temperature, the value of (V_m^E) becomes less negative. In the mixtures, negative V_m^E values can be due to the unlike interactions and also the placement of small molecules in spaces between polymer chains (compression effect). The positive values of V_m^E are characteristic of Van der Waals interactions between molecules. In the ZrO_2–PPG nanofluid system, there are different interactions between unlike molecules (polymer molecules and nanoparticles), and Van der Waals interactions between (polymer–polymer) and (nanoparticle–nanoparticle), while the similar interactions of nanoparticles together cause the agglomeration phenomenon. In the ZrO_2–PPG system, V_m^E is negative generally, so it can be concluded that the unlike interactions are dominant and also nanoparticles accommodation in the voids provided by the polymer.

According to Table 1 and Fig. 6(c) it can be seen that the V_m^E for the ZrO_2–H_2O–PVP is negative and becomes more negative in dilute areas and becomes positive with increasing the concentration of nanoparticles, which shows that there are interactions between nanoparticles and base fluid in the dilute regions, and with increasing in the concentration of nanoparticles, the amount of Van der Waals forces increases and the nanoparticles become agglomeration in the base fluid. The performance of the molar volume is related to the interactions between the hydrogen atoms of the H_2O and the oxygen atoms of PVP, which has a nitrogen molecule in its structure and has the ability to form a strong hydrogen bond with H_2O. It can also be seen that with the increasing in the temperature, the V_m^E value becomes more negative, which can be related to the effect of polymer compression, which breaks the long polymer chains and collapses its molecular structure with the increase in temperature. Nanoparticles come out of the compressed state and the interaction of nanoparticles with each other breaks down and they interact more with H_2O and PVP.[49–51]

It is also evident from Table 1 and Fig. 6(e) that V_m^E is negative for ZrO_2–H_2O nanofluid system and increases and becomes positive with increasing the concentration of nanoparticles; it can be concluded that in the ZrO_2–H_2O nanofluid system, small H_2O molecules create hydrogen bonds with each other and trap nanoparticles in the holes in the solution, but due to the high molecular mass of ZrO_2 nanoparticles, the hydrogen bonds between H_2O molecules is loosened and causes instability. By comparing the ZrO_2–H_2O and ZrO_2–H_2O–PVP systems, it can be indicated that V_m^E in the ZrO_2–H_2O system is negative and increases with the increase in the concentration of nanoparticles, while in the ZrO_2–H_2O–PVP system, it is negative and becomes more negative with increasing concentration in dilute regions and increases again with increasing nanoparticle concentration. In both systems, V_m^E becomes less negative with increasing the temperature. The effect of temperature in the ZrO_2–H_2O system is more noticeable than in the ZrO_2–H_2O–PVP system, and with increasing temperature, the amount of V_m^E decreases, which indicates that the number of weakened hydrogen bonds is more in the ZrO_2–H_2O system from ZrO_2–H_2O–PVP system.[52–56]

According to Table 1 and Fig. 6(d), the κ_s value for ZrO_2–H_2O–PVP system is positive in all concentrations and increases with increasing the concentration of nanoparticles and is almost constant in compact points. It decreases with increasing the temperature as it is evident from Table 1 and Fig. 6(f) that the κ_s for the ZrO_2–H_2O system increases with the increase in the concentration of nanoparticles and has almost a constant value in all areas and decreases with the increase in the temperature. In all studied nanofluids and at all temperatures, the isentropic compressibility has positive values, which indicates the existence of a regular molecular structure due to the presence of

Open Access Article. Published on 22 October 2024. Downloaded on 5/3/2026 10:35:04 AM. This article is licensed under a Creative Commons Attribution-NonCommercial 3.0 Unported Licence.

Table 1 Density (d), excess molar volume (V_m^E), viscosity (η), speed of sound (u), isentropic compressibility (κ_s), for nanofluid of ZrO_2 nanoparticles dispersed in PPG, PVP–H_2O, and H_2O at different temperatures[a]

$100 \times x_1$[b]	$100 \times \varphi_1$[c]	$10^{-3} \times d$ (kg m^{-3})	u (m s^{-1})	η (mPa s)	$10^6 \times V_m^E$ (m^3 mol^{-1})	$10^{12} \times \kappa_s$ (T Pa^{-1})
ZrO_2 nanoparticles dispersed in PPG						
$T = 293.15$ K						
0.2520	0.013	1.014337	1402.12	100.225	−0.038	501.473
0.5350	0.028	1.015157	1395.81	100.979	−0.068	505.608
0.9120	0.048	1.016418	1388.15	101.518	−0.172	510.569
1.2190	0.064	1.017508	1383.12	102.222	−0.278	513.739
1.6390	0.087	1.018998	1378.44	102.569	−0.417	516.477
3.5620	0.193	1.026107	1363.25	106.313	−1.100	524.392
5.7000	0.315	1.033569	1355.69	107.531	−1.574	526.429
$T = 298.15$ K						
0.2520	0.013	1.010667	1386.51	71.994	−0.183	514.690
0.5350	0.028	1.011509	1380.56	72.517	−0.222	518.704
0.9820	0.052	1.012819	1374.55	72.990	−0.347	522.573
1.2190	0.064	1.013891	1371.75	73.426	−0.447	524.154
1.6390	0.087	1.015499	1368.44	75.561	−0.633	525.859
3.5620	0.192	1.022647	1355.21	77.342	−1.336	532.428
5.7000	0.314	1.030289	1349.55	78.989	−1.879	532.921
$T = 308.15$ K						
0.2520	0.013	1.002978	1352.19	39.862	−0.496	545.297
0.5350	0.028	1.003792	1347.12	41.072	−0.526	548.964
0.9820	0.051	1.005127	1342.59	41.280	−0.664	551.940
1.2190	0.064	1.006219	1339.56	41.387	−0.774	553.839
1.6390	0.086	1.007790	1336.29	41.501	−0.950	555.685
3.5620	0.190	1.015008	1326.34	43.802	−1.696	560.042
5.7000	0.311	1.022781	1321.95	44.521	−2.301	559.484
$T = 318.15$ K						
0.2520	0.013	0.996634	1318.48	24.623	−1.071	577.188
0.5350	0.028	0.997400	1314.80	25.272	−1.082	579.978
0.9820	0.051	0.998628	1310.39	25.398	−1.178	583.170
1.2190	0.063	0.999735	1307.59	25.538	−1.296	585.022
1.6390	0.085	1.001199	1304.88	25.775	−1.432	586.595
3.5620	0.189	1.008329	1298.21	27.065	−2.156	588.448
5.7000	0.309	1.015912	1291.16	27.964	−2.700	590.451
ZrO_2 nanoparticles dispersed in PVP–H_2O (30% w/w)						
$T = 293.15$ K						
0.0031	0.003	1.062929	1639.58	60.502	−0.003	349.970
0.0071	0.006	1.063105	1638.85	61.162	−0.003	350.224
0.0100	0.009	1.063269	1638.44	61.322	−0.003	350.345
0.0130	0.011	1.063376	1638.25	61.621	−0.003	350.391
0.0180	0.015	1.063566	1637.98	61.745	−0.002	350.444
0.0260	0.022	1.063790	1637.65	62.069	0.000	350.511
0.0330	0.028	1.063999	1637.43	62.261	0.002	350.537
$T = 298.15$ K						
0.0031	0.003	1.061314	1643.24	49.419	−0.004	348.943
0.0071	0.006	1.061497	1642.69	49.701	−0.004	349.116
0.0100	0.009	1.061663	1642.47	49.793	−0.004	349.155
0.0130	0.011	1.061780	1642.32	50.034	−0.004	349.180
0.0180	0.015	1.061979	1642.05	50.326	−0.004	349.230
0.0260	0.022	1.062225	1641.89	51.251	−0.002	349.217
0.0330	0.028	1.062436	1641.74	51.789	0.000	349.211
$T = 308.15$ K						
0.0031	0.003	1.057130	1649.52	33.966	−0.005	347.661
0.0071	0.006	1.057316	1648.83	34.300	−0.005	347.891
0.0100	0.009	1.057479	1648.55	34.830	−0.005	347.956
0.0130	0.011	1.057591	1648.47	35.312	−0.005	347.953
0.0180	0.015	1.057796	1648.28	35.450	−0.005	347.965
0.0260	0.022	1.058056	1647.91	35.619	−0.003	348.036
0.0330	0.028	1.058285	1647.75	35.768	−0.002	348.028
$T = 318.15$ K						
0.0031	0.003	1.052388	1655.65	25.836	−0.006	346.647
0.0071	0.006	1.052571	1655.25	25.943	−0.006	346.754

© 2024 The Author(s). Published by the Royal Society of Chemistry

Open Access Article. Published on 22 October 2024. Downloaded on 5/3/2026 10:35:04 AM. This article is licensed under a Creative Commons Attribution-NonCommercial 3.0 Unported Licence.

Table 1 (*Contd.*)

$100 \times x_1$[b]	$100 \times \varphi_1$[c]	$10^{-3} \times d$ (kg m^{-3})	u (m s^{-1})	η (mPa s)	$10^6 \times V_m^E$ (m^3 mol^{-1})	$10^{12} \times \kappa_s$ (T Pa^{-1})
0.0100	0.009	1.052729	1654.90	26.106	−0.006	346.849
0.0130	0.011	1.052845	1654.73	26.267	−0.006	346.882
0.0180	0.015	1.053051	1654.48	26.422	−0.006	346.919
0.0260	0.022	1.053321	1654.16	26.541	−0.005	346.964
0.0330	0.028	1.053559	1653.88	26.677	−0.003	347.003
$100 \times x_1$[b]	$100 \times \varphi_1$[c]	$10^{-3} \times d$ (kg m^{-3})	u (m s^{-1})	$10^6 \times V_m^E$ (m^3 mol^{-1})		$10^{12} \times \kappa_s$ (T Pa^{-1})
ZrO_2 nanoparticles dispersed in H_2O						
$T = 293.15$ K						
0.1700	0.194	0.998418	1482.95	−0.002		455.444
0.2920	0.333	0.998443	1482.90	−0.001		455.463
0.3650	0.417	0.998464	1482.78	−0.001		455.527
0.5110	0.583	0.998505	1482.79	0.000		455.502
0.6080	0.694	0.998534	1482.59	0.000		455.612
0.7290	0.832	0.998572	1482.89	0.001		455.410
$T = 298.15$ K						
0.1700	0.194	0.997386	1496.98	−0.004		447.409
0.2920	0.333	0.997394	1497.08	−0.003		447.346
0.3650	0.417	0.997405	1496.92	−0.003		447.436
0.5110	0.583	0.997431	1496.87	−0.002		447.455
0.6080	0.694	0.997455	1496.70	−0.001		447.545
0.7290	0.832	0.997489	1496.91	−0.001		447.405
$T = 308.15$ K						
0.1700	0.194	0.994495	1519.73	−0.007		435.376
0.2920	0.333	0.994490	1519.75	−0.005		435.367
0.3650	0.417	0.994494	1519.65	−0.005		435.422
0.5110	0.583	0.994499	1519.59	−0.003		435.455
0.6080	0.694	0.994519	1519.41	−0.003		435.549
0.7290	0.832	0.994558	1519.73	−0.002		435.348
$T = 318.15$ K						
0.1700	0.194	0.990520	1536.19	−0.014		427.806
0.2920	0.333	0.990525	1536.33	−0.013		427.726
0.3650	0.417	0.990529	1536.12	−0.012		427.841
0.5110	0.583	0.990534	1535.98	−0.011		427.917
0.6080	0.694	0.990539	1535.85	−0.010		427.987
0.7290	0.832	0.990555	1536.02	−0.009		427.886

[a] The standard uncertainties for molality, temperature and pressure were $u(m) = 0.001$ mol kg^{-1}, $u(T) = 0.2$ K, $u(P) = 10.5$ h Pa, respectively with level of confidence 0.95. The standard combined uncertainty for viscosity was about, $u_c(\eta) = 0.02$ mPa s, for density were about, $u_c(d) = 0.06 \times 10^{-3}$ g cm^{-3}, and for speed of sound were about, $u_c(u) = 1.5$ m s^{-1} (level of confidence 0.68). [b] x_1: mole fraction of ZrO_2 nanoparticle. [c] φ_1: volume fraction of ZrO_2 nanoparticle.

strong hydrogen bonds. At high temperatures, hydrogen bonds are weakened and the coherent molecular structure collapses. The isentropic compressibility performance of the studied nanofluids can be shown as follows:

$$\kappa_s(ZrO_2\text{–PPG}) > \kappa_s(ZrO_2\text{–}H_2O) > \kappa_s(ZrO_2\text{–}H_2O\text{–PVP30\%})$$

The studies conducted on excess molar volume (V_m^E) and isentropic compressibility (κ_s) and the obtained results confirm the results of UV-vis spectroscopy.

3.4. Viscosity results

In order to ensure the accuracy of the data obtained from the capillary viscometer, the viscosity of ZrO_2–PPG and ZrO_2–H_2O–PVP nanofluids was also measured over the time and the changes of $\eta/\eta_{basefluid}$ for these nanofluids are shown according to time in Fig. 7.

Fig. 7 shows the repeatability of viscosity data in terms of time, which is a confirmation of the suitability of capillary viscometers for these measurements. According to the Table 1, the viscosity of ZrO_2–PPG and ZrO_2–H_2O–PVP nanofluids increased with increasing the concentration of nanoparticles and decreased with increasing temperature. It should be noted that, for both mentioned systems, the effect of temperature on the viscosity of nanofluids is more significant than the effect of increasing concentration. In the results reported in a study conducted on the viscosity of the ZrO_2–H_2O system, it has been observed that the viscosity of the mentioned nanofluid is affected by the concentration of nanoparticles and negligible change in viscosity is seen with the temperature change.

Open Access Article. Published on 22 October 2024. Downloaded on 5/3/2026 10:35:04 AM.
This article is licensed under a Creative Commons Attribution-NonCommercial 3.0 Unported Licence.

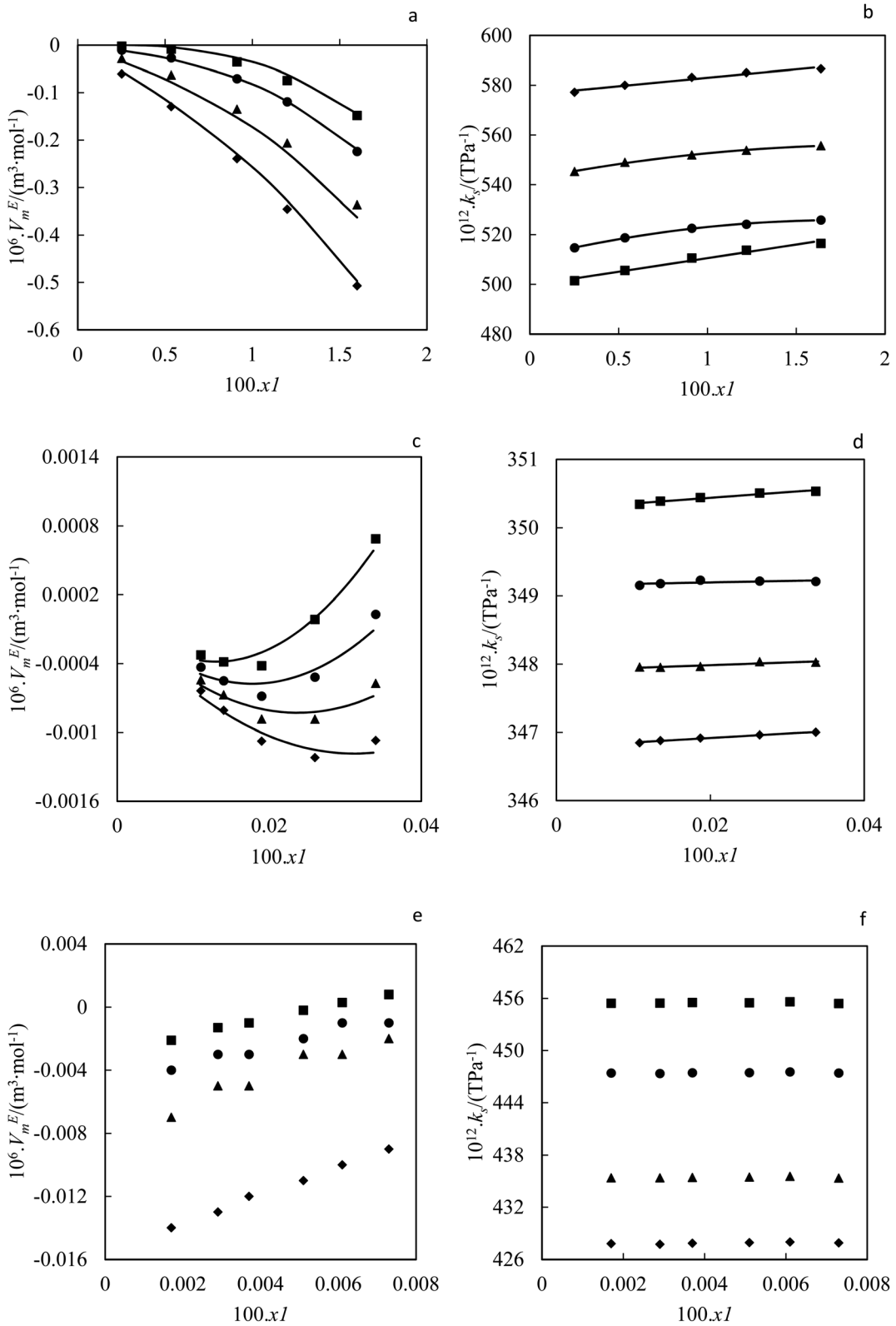

Fig. 6 Excess molar volume (a) and (b) isentropic compressibility in terms of nanoparticle mole fraction for ZrO_2–PPG system at T = ((■) 293.15, (●) 298.15, (▲) 308.15, (◆) 318.15) K in comparison with (—) polynomial equation; excess molar volume (c) and (d) isentropic compressibility in terms of nanoparticle mole fraction for ZrO_2–H_2O–PVP system at T = ((■) 293.15, (●) 298.15, (▲) 308.15, (◆) 318.15) K compared to (—) polynomial equation; experimental data of (e) excess molar volume and (f) isentropic compressibility in terms of nanoparticle mole fraction for ZrO_2–H_2O system at T = ((■) 293.15, (●) 298.15, (▲) 308.15, (◆) 318.15) K.

© 2024 The Author(s). Published by the Royal Society of Chemistry

Open Access Article. Published on 22 October 2024. Downloaded on 5/3/2026 10:35:04 AM.
This article is licensed under a Creative Commons Attribution-NonCommercial 3.0 Unported Licence.

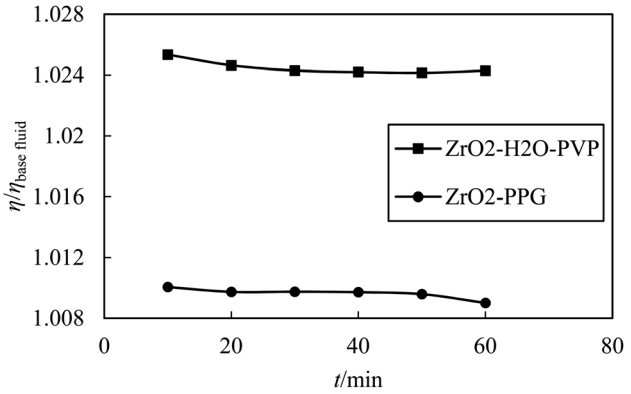

Fig. 7 Experimental viscosity ratio $\eta/\eta_{basefluid}$ plotted against time (t min^{-1}) for of ZrO_2 in PPG and H_2O–PVP.

4. Correlation

The V_m^E values of nanofluid systems were correlated by Redlich–Kister, Ott[57] and polynomial equation at each temperature. These equations listed respectively in eqn (5)–(7). In the polynomial eqn (7), A_h is the polynomial coefficient and $h + 1$ is the number of polynomial coefficients. In this research, the V_m^E values are fitted by the mentioned equations by two methods. Each of the equations are given a temperature dependence by writing each of the parameters as $A_0 + \frac{A_1}{T}$, and two methods are tried in fitting the data. In the first method, the usual fitting method was used, and in the second method, the fitting was done by dividing the main equation into x_1x_2 . The efficiency of the equations was studied by comparing the standard deviation obtained from the excess molar volumes and the density of the samples. Fitting the V_m^E values was done by using the mentioned equations and using two fitting methods in each equation. Due to the lack of acceptable results from the fitting of the V_m^E values for the ZrO_2–H_2O system, the fitting data of this system was not studied. In Table 2, the standard deviation related to fitting the V_m^E values and density data of the ZrO_2–PPG and ZrO_2–H_2O–PVP using the mentioned equations are reported. According to the results of Table 2, it can be concluded that the standard deviation related to the polynomial eqn (7), in fitting the data in both systems are acceptable while the second method has a better efficiency in fitting than the first method.

In Table S3† the standard deviations obtained from fitting the V_m^E values and density data are reported for ZrO_2–PPG and ZrO_2–H_2O–PVP systems, respectively, using temperature dependent equations. According to these tables, the efficiency of the polynomial equation with temperature dependency for

Table 2 Standard deviations (σ) from fitting the excess molar volume (V_m^E) values in eqn (5)–(7) for ZrO_2–PPG and ZrO_2–H_2O–PVP at different temperatures

	Ott *et al.*		Redlich–Kister		Polynomial	
	Method 1	Method 2	Method 1	Method 2	Method 1	Method 2
ZrO_2–PPG						
T = 293.15 K						
$10^3 \times \sigma$ (V_m^E/(cm^3 mol^{-1}))	8.7	1.8	20.4	10.0	7.4	1.7
$10^4 \times \sigma$ (d/g cm^{-3})	6.1	4.8	6.1	5.0	6.1	4.8
T = 298.15 K						
$10^3 \times \sigma$ (V_m^E/(cm^3 mol^{-1}))	5.8	0.9	95.5	26.2	21.9	0.8
$10^4 \times \sigma$ (d/g cm^{-3})	10.2	7.9	10.2	7.2	10.2	7.9
T = 308.15 K						
$10^3 \times \sigma$ (V_m^E/(cm^3 mol^{-1}))	7.4	1.7	65.0	5.2	64.5	1.6
$10^4 \times \sigma$ (d/g cm^{-3})	17.6	13.8	17.6	13.8	17.6	13.8
T = 318.15 K						
$10^3 \times \sigma$ (V_m^E/(cm^3 mol^{-1}))	4.9	3.0	553.7	5.6	142.0	2.9
$10^4 \times \sigma$ (d/g cm^{-3})	30.5	24.2	30.0	24.2	30.2	24.2
Overall ($10^3 \times \sigma$ (V_m^E/(cm^3 mol^{-1})))	6.7	1.9	178.7	11.8	58.9	1.8
Overall ($10^4 \times \sigma$ (d/g cm^{-3}))	16.1	12.7	16.0	12.6	16.0	12.7
ZrO_2–H_2O–PVP (30% w/w)						
T = 293.15 K						
$10^4 \times \sigma$ (V_m^E/(cm^3 mol^{-1}))	8.8	0.3	4.7	2.3	4.0	0.7
$10^4 \times \sigma$ (d/g cm^{-3})	1.0	0.8	1.3	0.8	1.0	0.8
T = 298.15 K						
$10^4 \times \sigma$ (V_m^E/(cm^3 mol^{-1}))	3.6	4.2	3.9	2.0	3.9	0.9
$10^4 \times \sigma$ (d/g cm^{-3})	1.4	1.1	1.4	1.2	1.4	1.2
T = 308.15 K						
$10^4 \times \sigma$ (V_m^E/(cm^3 mol^{-1}))	1.4	1.4	6.4	1.2	5.2	0.7
$10^4 \times \sigma$ (d/g cm^{-3})	1.8	1.5	1.8	1.5	40.5	1.5
T = 318.15 K						
$10^4 \times \sigma$ (V_m^E/(cm^3 mol^{-1}))	0.9	1.0	8.9	0.7	6.2	0.6
$10^4 \times \sigma$ (d/g cm^{-3})	2.3	1.9	2.3	1.9	2.3	1.9
Overall ($10^4 \times \sigma$ (V_m^E/(cm^3 mol^{-1})))	3.6	1.7	5.9	1.5	4.8	0.7
Overall ($10^4 \times \sigma$ (d/g cm^{-3}))	1.6	1.3	1.7	1.3	11.3	1.3

Open Access Article. Published on 22 October 2024. Downloaded on 5/3/2026 10:35:04 AM.
This article is licensed under a Creative Commons Attribution-NonCommercial 3.0 Unported Licence.

Table 3 Excess molar volume (V_m^E) parameters of eqn (5)–(7) using the first fitting method for ZrO_2–PPG and ZrO_2–H_2O–PVP systems at different temperatures

ZrO_2–PPG – eqn (5)				
	$10^{-5} \times A_0$	$10^{-5} \times A_1$	$10^{-5} \times A_2$	σ
$T = 293.15$ K				
$10^6 \times V_m^E/(m^3\ mol)^{-1}$	0.07845	0.166	0.08751	0.020
$T = 298.15$ K				
$10^6 \times V_m^E/(m^3\ mol)^{-1}$	−0.5284	−1.083	−0.5554	0.095
$T = 308.15$ K				
$10^6 \times V_m^E/(m^3\ mol)^{-1}$	−1.64	−3.376	−1.738	0.065
$T = 318.15$ K				
$10^6 \times V_m^E/(m^3\ mol)^{-1}$	−3.881	−7.996	−4.12	0.553

ZrO_2–H_2O–PVP30% – eqn (5)				
	$10^{-4} \times A_0$	$10^{-7} \times A_1$	$10^{-4} \times A_2$	$\sigma \times 10^4$
$T = 293.15$ K				
$10^6 \times V_m^E/(m^3\ mol)^{-1}$	3.431	−2.014	−3.435	4.70
$T = 298.15$ K				
$10^6 \times V_m^E/(m^3\ mol)^{-1}$	3.8	−2.163	−3.805	3.90
$T = 308.15$ K				
$10^6 \times V_m^E/(m^3\ mol)^{-1}$	4.031	2.072	−4.037	6.47
$T = 318.15$ K				
$10^6 \times V_m^E/(m^3\ mol)^{-1}$	4.361	−2.884	−4.368	8.97

ZrO_2–PPG – eqn (6)							
	A_0	A_1	A_2	A_3	A_4	A_5	σ
$T = 293.15$ K							
$10^6 \times V_m^E/(m^3\ mol)^{-1}$	1.164	−368.304	0.00074	−0.931	0.001375	359.181	0.008
$T = 298.15$ K							
$10^6 \times V_m^E/(m^3\ mol)^{-1}$	607.679	−62.253	−112.654	−106.015	−25.958	97.299	0.005
$T = 308.15$ K							
$10^6 \times V_m^E/(m^3\ mol)^{-1}$	545.88	−365.089	−104.117	283.253	−7.734	−358.568	0.007
$T = 318.15$ K							
$10^6 \times V_m^E/(m^3\ mol)^{-1}$	492.221	−519.075	−445.575	40.94	1790	−1 990 000	0.004

ZrO_2–H_2O–PVP30% – eqn (6)							
	A_0	A_1	A_2	$10^{-4} \times A_3$	A_4	$10^{-3} \times A_5$	σ
$T = 293.15$ K							
$10^6 \times V_m^E/(m^3\ mol)^{-1}$	1.757	1.167	39.417	3.4	614.014	−3.469	8.87
$T = 298.15$ K							
$10^6 \times V_m^E/(m^3\ mol)^{-1}$	334.554	−237.219	−248.974	0.0836299	40.959	−0.044249	3.64
$T = 308.15$ K							
$10^6 \times V_m^E/(m^3\ mol)^{-1}$	8480	1896	−2007	0.495	−4.152	−0.4953	1.41
$T = 318.15$ K							
$10^6 \times V_m^E/(m^3\ mol)^{-1}$	7742	1586	−1704	0.3406	−6.208	−0.3407	0.92

ZrO_2–PPG – eqn (7)				
	A_0	$10^{-4} \times A_1$	$10^{-6} \times A_2$	σ
$T = 293.15$ K				
$10^6 \times V_m^E/(m^3\ mol)^{-1}$	−5.918	−0.18	0.03501	0.007
$T = 298.15$ K				
$10^6 \times V_m^E/(m^3\ mol)^{-1}$	−70.656	0.5546	−0.2222	0.021
$T = 308.15$ K				
$10^6 \times V_m^E/(m^3\ mol)^{-1}$	−200.6	1.999	−0.695	0.064
$T = 318.15$ K				
$10^6 \times V_m^E/(m^3\ mol)^{-1}$	−445.801	4.866	−1.648	0.142

© 2024 The Author(s). Published by the Royal Society of Chemistry

Open Access Article. Published on 22 October 2024. Downloaded on 5/3/2026 10:35:04 AM. This article is licensed under a Creative Commons Attribution-NonCommercial 3.0 Unported Licence.

Table 3 (*Contd.*)

ZrO_2–H_2O–PVP30% – eqn (7)				
	A_0	$10^{-5} \times A_1$	$10^{-8} \times A_2$	$10^4\ \sigma$
$T = 293.15$ K				
$10^6 \times V_m^E/(m^3\ mol)^{-1}$	−38.934	1.373	2.894	4.07
$T = 298.15$ K				
$10^6 \times V_m^E/(m^3\ mol)^{-1}$	−49.989	1.521	3.363	3.90
$T = 308.15$ K				
$10^6 \times V_m^E/(m^3\ mol)^{-1}$	−58.307	1.614	2.09	5.27
$T = 318.15$ K				
$10^6 \times V_m^E/(m^3\ mol)^{-1}$	−67.084	1.746	1.796	6.21

both systems and using both methods is better than the Redlich–Keister and Ott equations with temperature dependency. Also, the efficiency of the second method in fitting of the V_m^E values and density data was better than the first method in all equations. Therefore, according to the results of the standard deviation of all systems and all temperatures, the efficiency of the polynomial equation with the second method and temperature dependency is better than other methods. The parameters of Redlich-Kister, Ott *et al.* and polynomial equations, using the first fitting method are also reported in Table 3.

Also, the parameters of the Redlich–Kister, Ott *et al.* and polynomial equations using the second fitting method are reported in Table 4.

Continuous lines in Fig. 6(a) and (c) correspond to this equation. The parameters of the polynomial equation with temperature dependency and using the second fitting method, for ZrO_2–PPG and ZrO_2–H_2O–PVP systems are reported in Table S4.† The continuous lines in Fig. S1(a) and (b)† for ZrO_2–PPG and ZrO_2–H_2O–PVP systems are in accordance with this model, which is compared with the obtained experimental data. The parameters of Redlich–Kister,[58,59] Ott[57] and polynomial temperature dependent equations using the first fitting method, are reported in Tables S5, S6, and S7† respectively. Also, the parameters of the temperature dependent equations of Redlich–Kister[58,59] and Ott[57] using the second fitting method are reported in Tables S8 and S9.† The isentropic compressibility (κ_s) data of the considered systems were fitted by the polynomial equation. The parameters obtained from this equation are reported in Table 4 for ZrO_2–PPG and ZrO_2–H_2O–PVP nanofluids. Continuous lines in Fig. 6(b) and (d) correspond to this equation. These figures and Table 4 show that the efficiency of the polynomial equation is acceptable.

$$V_m^E = x_1 x_2 \sum_{h \geq 0} A_h (x_1 - x_2)^h \tag{5}$$

$$V_m^E = x_2(1 - x_2)\left[\exp(-\gamma x_2)\sum_{I=0}^{1} B_1 (1 - 2x_2)^I + (1 - \exp(-\gamma x_2))\sum_{I=0}^{3} (1 - 2x_2)^I\right] \tag{6}$$

$$V_m^E = \sum_{h \geq 0} x_1 x_2 A_h (x_1)^h \tag{7}$$

It is important to fit viscosity data of nanofluids by considering the dependence of concentration and temperature simultaneously. In some equations, the temperature dependency is only considered. The equations with only a concentration dependency are alternatively used for predicting the viscosity of nanofluids systems at each temperature. Models that altogether consider temperature and concentration dependence have many parameters. In recent years, the Eyring-NRTL model has been used with good efficiency in fitting the viscosity data. In this research, the effectiveness of the mentioned model and the new Eyring-mNRF model in fitting the viscosity data of ZrO_2–PPG and ZrO_2–H_2O–PVP nanofluids systems have been investigated. The Eyring-NRTL equation is as follows:[14,60–63]

$$n(\eta V) = \sum_{I=1}^{n} \phi_I \ln(\eta_I V_I) + \sum_{I=1}^{n} \phi_I \frac{\sum_{J=1}^{n} \phi_J A_{JI} G_{JI}}{\sum_{J=1}^{n} \phi_J G_{JI}} \tag{8}$$

$$A_{JI} = a_{JI} + b_{JI} T \tag{9}$$

$$G_{JI} = \exp\left(-\frac{\alpha A_{JI}}{RT}\right) \tag{10}$$

V and V_I are the molar volume of the nanofluid and component I, φ_I is the volume fraction of component I, equal to $\frac{x_I V_I}{\sum_{J=1}^{3} (x_J V_J)}$ in which x_I is the mole fraction of component I. The T is temperature and R is the universal constant of gases; a_{JI} and b_{JI} are empirical parameters of the Eyring-NRTL model. The a is the non-randomness factor which was set to 0.2 in this work.- The Eyring-mNRF model is represented by the following equation:[14,60–63]

$$\ln(\eta V) = \sum_{I=1}^{n} X_I \ln(\eta_I V_I) + \frac{N}{N_s}\sum_{w''} x_{w''} \sum_{j}\sum_{w'}\sum_{w} \frac{X_w \frac{\lambda_{jw,w'w}}{RT}\left(-X_w \Gamma_{w'w} - X_j \Gamma_{w'w} + 1\right)}{X_j + X_w} + \sum_{w''}\sum_{p} r_{p,w''} x_p \sum_{j}\sum_{s''}\sum_{s'} \frac{X_{s'} \frac{\lambda_{s''s'js'}}{RT}\left(X_{s'} \Gamma_{s''s'} - X_j \Gamma_{s''s'} - 1\right)}{X_{s'} + X_j} \tag{11}$$

Open Access Article. Published on 22 October 2024. Downloaded on 5/3/2026 10:35:04 AM. This article is licensed under a Creative Commons Attribution-NonCommercial 3.0 Unported Licence.

Table 4 Excess molar volume (V_m^E) parameters of eqn (5)–(7) using the second fitting method for ZrO_2–PPG and ZrO_2–H_2O–PVP through utilization of Redlich–Kister and Ott equations at different temperatures

ZrO_2–PPG – eqn (5)

	$10^{-3}A_0$	A_1	$10^{-3}A_2$	σ
$T = 293.15$ K				
$10^6 \times V_m^E$/m^3 mol^{-1}	−6.097	−12090	−5.992	0.010
$T = 298.15$ K				
$10^6 \times V_m^E$/m^3 mol^{-1}	−7.758	−15410	−7.658	0.026
$T = 308.15$ K				
$10^6 \times V_m^E$/m^3 mol^{-1}	−0.206268	−0.0002367	0.197979	0.005
$T = 318.15$ K				
$10^6 \times V_m^E$/m^3 mol^{-1}	−7.764	−15450	−7.709	0.005

ZrO_2–H_2O–PVP30% –eqn (5)

	$10^{-3}A_0$	A_1	$10^{-3}A_2$	$10^4\sigma$
$T = 293.15$ K				
$10^6 \times V_m^E$/m^3 mol^{-1}	5.657	7.866	−5.656	2.36
$T = 298.15$ K				
$10^6 \times V_m^E$/m^3 mol^{-1}	4.57	7.637	−4.568	2.02
$T = 308.15$ K				
$10^6 \times V_m^E$/m^3 mol^{-1}	3.667	7.405	−3.667	1.25
$T = 318.15$ K				
$10^6 \times V_m^E$/m^3 mol^{-1}	3.044	7.439	−3.044	0.73

ZrO_2–PPG – eqn (6)

	A_0	A_1	A_2	A_3	A_4	A_5	σ
$T = 293.15$ K							
$10^6 \times V_m^E$/m^3 mol^{-1}	−18.656	−703.285	772.435	−69.78	0.526	0.245	0.001
$T = 298.15$ K							
$10^6 \times V_m^E$/m^3 mol^{-1}	−69.882	−28.451	25.213	−1.785	0.686	1.38	0.000
$T = 308.15$ K							
$10^6 \times V_m^E$/m^3 mol^{-1}	−68.041	−13.028	8.654	−8.746	−1.871	5.232	0.001
$T = 318.15$ K							
$10^6 \times V_m^E$/m^3 mol^{-1}	−87.469	−1.385	−0.724	−17.796	−5.389	2.326	0.003

ZrO_2–H_2O–PVP30% – eqn (6)

	A_0	A_1	A_2	$10^{-4}A_3$	A_4	$10^{-3}A_5$	σ
$T = 293.15$ K							
$10^6 \times V_m^E$/m^3 mol^{-1}	−3900	57.508	−53.281	−0.2153	−28.07	2.173	0.37
$T = 298.15$ K							
$10^6 \times V_m^E$/m^3 mol^{-1}	−1977	706.587	−681.511	−1.482	−20.593	14.81	4.26
$T = 308.15$ K							
$10^6 \times V_m^E$/m^3 mol^{-1}	0.222	223.192	−43.175	0.3742	−0.528	−3.659	1.45
$T = 318.15$ K							
$10^6 \times V_m^E$/m^3 mol^{-1}	0.558	−7.376	−10.963	0.305	0.133	−3.039	1.04

Table 4 (*Contd.*)

ZrO_2_PPG – eqn (7)

	A_0	A_1	A_2	σ
$T = 293.15$ K				
$10^6 \times V_m^E$/m^3 mol^{-1}	−0.012	−210.271	$-2.396.10^4$	0.00179
κ_s/(T Pa^{-1})	$4.999.10^{-7}$	$1.188.10^{-6}$	$-1.282.10^{-5}$	0.842
$T = 298.15$ K				
$10^6 \times V_m^E$/m^3 mol^{-1}	−3.324	−193.136	$-3.063.10^4$	0.00089
κ_s/(T Pa^{-1})	510.745	$1.731.10^3$	$-4.975.10^4$	0.177
$T = 308.15$ K				
$10^6 \times V_m^E$/m^3 mol^{-1}	−10.146	−242.146	$-2.906.10^4$	0.0045
κ_s/(T Pa^{-1})	542.137	$1.41.10^3$	$-3.591.10^4$	0.176
$T = 318.15$ K				
$10^6 \times V_m^E$/m^3 mol^{-1}	−23.497	−62.186	$-3.084.10^4$	0.00294
κ_s/(T Pa^{-1})	576.161	683.678	−1.012	0.630

ZrO_2–H_2O–PVP30% – eqn (7)

	A_0	A_1	A_2	$10^4\ \sigma$
$T = 293.15$ K				
$10^6 \times V_m^E$/m^3 mol^{-1}	−5.892	$2.263.10^4$	11.283	0.72
κ_s/(T Pa^{-1})	350.274	832.154	$3.125.10^{-4}$	0.015
$T = 298.15$ K				
$10^6 \times V_m^E$/m^3 mol^{-1}	−6.49	$1.828.10^4$	9.428	0.91
κ_s/(T Pa^{-1})	349.154	217.412	1.065	0.020
$T = 308.15$ K				
$10^6 \times V_m^E$/m^3 mol^{-1}	−6.98	$1.468.10^4$	7.762	0.73
κ_s/(T Pa^{-1})	347.905	400.153	1.122	0.015
$T = 318.15$ K				
$10^6 \times V_m^E$/m^3 mol^{-1}	−7.595	$1.218.10^4$	6.624	1.92
κ_s/(T Pa^{-1})	346.788	652.935	1.22	0.007

$$\Gamma_{is'} = \frac{\beta_{is',ws'}}{\sum_{w'} X_{w'}\beta_{w'i,ws'} + \sum_{s''} X_{s''}\beta_{is'',ws'}} \quad (12)$$

$$\Gamma_{iw} = \frac{1}{\sum_{w'} X_{w'}\beta_{iw',iw} + \sum_{s'} X_{s'}\beta_{s'i,iw}} \quad (13)$$

$$\lambda_{ij,kl} = \lambda_{ij,lk} = \lambda_{ji,kl} = \lambda_{ji,lk} = -\lambda_{kl,ij} = -\lambda_{lk,ij} = -\lambda_{kl,ji} = -\lambda_{lk,ji} \quad (14)$$

$$\omega_{ij,kl} = \omega_{ij,lk} = \omega_{ji,kl} = \omega_{ji,lk} = -\omega_{kl,ij} = -\omega_{lk,ij} = -\omega_{kl,ji} = -\omega_{lk,ji} \quad (15)$$

$$\beta_{ij,lk} = \exp\left(-\frac{\lambda_{ij,lk}}{ZRT} + \frac{\omega_{ij,lk}}{RT}\right) \quad (16)$$

$$X_s = \frac{x_2}{\sum_{I=1}^{3} r_I x_I} \quad (17)$$

where, $r_{p,w''}$ approximates the ratio of the molar volume of the polymer (p) and corresponding solvent molecule (w''). N is the total number of polymers, nanoparticles and solvents. Subscripts s, s', s'' represented polymer monomers,

© 2024 The Author(s). Published by the Royal Society of Chemistry

Open Access Article. Published on 22 October 2024. Downloaded on 5/3/2026 10:35:04 AM. This article is licensed under a Creative Commons Attribution-NonCommercial 3.0 Unported Licence.

Table 5 Eyring-NRTL and Eyring-mNRF model parameters along with standard deviation (σ) for ZrO_2–PPG and ZrO_2–H_2O–PVP

ZrO_2–PPG					
Eyring-NRTL	a_{12}	b_{12}	a_{21}	b_{21}	σ (η/mPa s)
	−8168.231	−33.02	83 288.78	−7.639	0.001
Eyring-mNRF	λ_{1sss}	λ_{11s1}	ω_{1sss}	ω_{11s1}	σ (η/mPa s)
	11 078 397.892	−13 187 248.059	1 382 771.024	81 508.806	0.001
ZrO_2–H_2O–PVP					
Eyring-NRTL	a_{12}	b_{12}	a_{21}	b_{21}	σ (η/mPa s)
	−0.107	−37.986	242.359	94.6	0.001
Eyring-mNRF	λ_{1sss}	λ_{11s1}	ω_{1sss}	ω_{11s1}	σ (η/mPa s)
	−37 855.873	−65 583 122.907	7443.86	−8 191 662.783	0.001

nanoparticle and solvent moles, w, w', w'' show the solvent molecules; i, j, k and l stand for segments of polymer chain, solvent molecules and nanoparticles. The $\lambda_{ij,lk}$ and $w_{ij,lk}$ are the parameters of the Eyring-mNRF model. Z is the non-random factor which was set to 8 in this work.

Parameters of the Eyring-mNRF model along with the standard deviation resulting from this model and also the Eyring-NRTL model resulting from fitting the viscosity data of the ZrO_2–PPG and ZrO_2–H_2O–PVP nanofluids systems are shown in Table 5. In order to observe the performance of the Eyring-NRTL and Eyring-mNRF models in a better manner, the experimental and calculated viscosity values with these two models are shown in Fig. 8.

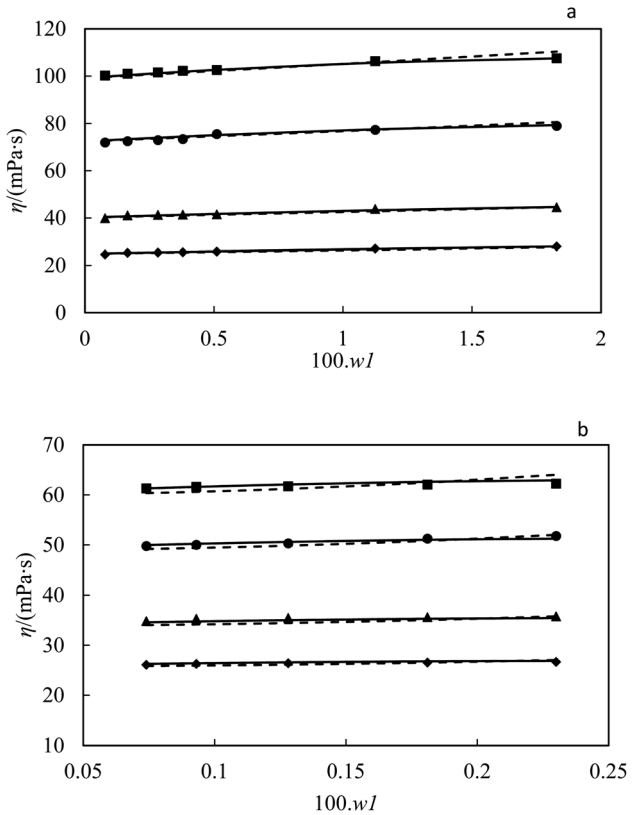

Fig. 8 Viscosity by weight fraction for nanofluid (a) ZrO_2–PPG and (b) ZrO_2–H_2O–PVP at T = ((■) 293.15, (●) 298.15, (▲) 308.15, (◆) 318.15) K compared to (—) NRTL and (——) mNRF equation.

As can be seen from Table 5, the performance of both Eyring-NRTL and Eyring-mNRF models is good in fitting the viscosity data of both systems.

5. Prediction

The viscosity data of nanofluids containing two components can be predicted by well-known equations such as Einstein (18), Brinkman (19), Lundgren (20) and Batchelor (21) models. These equations are as follows:

$$\eta = \eta_2(1 + 2.5\varphi_1) \tag{18}$$

$$\eta = \eta_2\left(\frac{1}{1-\varphi_1^{2.5}}\right) \tag{19}$$

$$\eta = \eta_2\left(1 + 2.5\varphi_1 + \frac{25}{4}{\varphi_1}^2 + f\left({\varphi_1}^3\right)\right) \tag{20}$$

$$\eta = \eta_2(1 + 2.5\varphi_1 + 6.2{\varphi_1}^2) \tag{21}$$

In eqn (18), the η and η_2 are the viscosity of nanofluid and viscosity of base fluid, respectively and in eqn (20), $f({\varphi_1}^3)$ is the Taylor series for volume fraction of nanofluid (φ_1). The Taylor series is as follows eqn (22):[14]

$$f({\varphi_1}^3) = 0.01 + 0.0003(\varphi_1 - 0.01) + 0.03(\varphi_1 - 0.01)^2 + (\varphi_1 - 0.01)^3 \tag{22}$$

In this research, the viscosity data of ZrO_2–PPG and ZrO_2–H_2O–PVP nanofluids have been predicted by these equations at four temperatures; the results are reported in Table 6. This table show the good performance of the mentioned models and especially the Lundgren model eqn (20) in predicting the viscosity data of ZrO_2–PPG and ZrO_2–H_2O–PVP in the dilute concentration region.

The good performance of the Lundgren model eqn (20) in predicting the viscosity data of ZrO_2–PPG and ZrO_2–H_2O–PVP nanofluids, particularly in the dilute concentration region, can be attributed to several key factors. This model effectively accounts for the interaction between dispersed nanoparticles and the base fluid, making it highly suitable for capturing the behavior of nanofluids in dilute concentrations where particle–

© 2024 The Author(s). Published by the Royal Society of Chemistry

Open Access Article. Published on 22 October 2024. Downloaded on 5/3/2026 10:35:04 AM. This article is licensed under a Creative Commons Attribution-NonCommercial 3.0 Unported Licence.

Table 6 Standard deviations (σ (η/mPa s)) and absolute average relative deviations (AARD) obtained from prediction of viscosity values of nanofluid of ZrO_2–PPG and ZrO_2–H_2O–PVP with Einstein[64–66] (eqn (18)), Brinkman[65,67] (eqn (19)), Lundgren[68] (eqn (20)) and Batchelor[69] (eqn (21)) models

	Einstein model		Brinkman model		Lundgren model		Batchelor model	
T/K	σ	100 *AARD*	σ	100 *AARD*	σ	100 *AARD*	σ	100 *AARD*
ZrO_2–PPG								
293.15	4.227	3.371	4.584	3.624	3.440	2.406	4.225	3.369
298.15	3.032	2.553	3.292	2.807	2.615	1.580	3.030	2.552
308.15	2.159	3.763	2.304	4.013	1.875	2.802	2.159	3.762
318.15	1.416	3.681	1.507	3.930	1.254	2.719	1.416	3.680
ZrO_2–H_2O–PVP								
293.15	1.926	3.072	1.966	3.132	1.339	2.103	1.926	3.072
298.15	1.952	3.541	1.985	3.601	1.513	2.577	1.952	3.541
308.15	1.618	4.478	1.641	4.537	1.289	3.523	1.618	4.477
318.15	0.744	2.716	0.761	2.777	0.501	1.744	0.744	2.716

particle interactions are minimal. In this regard, viscosity is mainly influenced by individual nanoparticles, and the Lundgren model is specifically designed to handle such conditions. Additionally, the model likely considers the shear-thinning behavior of nanofluids like ZrO_2–PPG and ZrO_2–H_2O–PVP, which further enhances its adaptability to different flow dynamics at low concentrations. Moreover, the model incorporates temperature sensitivity, enabling it to accurately reflect the temperature-dependent viscosity of nanofluids, which is crucial for predicting viscosity across various temperatures. These factors collectively explain the model's superior accuracy in predicting viscosity under these conditions.

6. Conclusions

In these research, ZrO_2–PPG nanofluid was found to be the most stable among the studied nanofluids, remaining stable for over a month. ZrO_2–H_2O nanofluid was stable for 24 hours, while ZrO_2–PPG–H_2O nanofluid was unstable at different ratios. The addition of water to the ZrO_2–PPG system increased interactions between the polymer and water, leading to nanoparticle agglomeration. The size of nanoparticles in the stable ZrO_2–PPG nanofluid was found to be larger than the initial size. Excess molar volume and isentropic compressibility were calculated from density, speed of sound, and viscosity measurements. Negative excess molar volume values suggested unlike interactions and compression effects, while positive values indicated Van der Waals interactions. ZrO_2–H_2O nanofluid exhibited interactions between water molecules and nanoparticles. ZrO_2–H_2O–PVP nanofluid with 30% polymer was the most stable, with dominant unlike interactions in dilute and semi-dilute regions and Van der Waals forces in concentrated regions. Redlich-Kister, Ott, and polynomial equations were used to fit excess molar volume data, the polynomial equation with temperature dependence performing best. Eyring-NRTL and Eyring-mNRF models were used to correlate viscosity data, with both models showing good performance. Einstein, Brinkman, Lundgren, and Batchelor models were used to predict viscosity data of ZrO_2–PPG and ZrO_2–H_2O–PVP nanofluids at four temperatures.

There is minimal limitation about the focus on potential industrial applications or scalability, which is critical for determining the real-world relevance of these findings. The findings may apply to other nanofluid systems that is not investigated yet. Future research on ZrO_2-based nanofluids could focus on enhancing the stability of ZrO_2–H_2O and ZrO_2–PPG–H_2O systems by exploring additives or surface modifications to prevent nanoparticle agglomeration. Further studies on the interaction mechanisms, particularly in mixed fluid systems, can provide deeper insights into optimizing nanofluid properties for various applications. Advanced modeling approaches, integrating temperature dependence and particle dynamics, could refine predictions of viscosity and other thermophysical properties. Additionally, improving the stability and performance of these nanofluids could enhance their potential in heat transfer and industrial applications.

Data availability

Data are available upon request from the authors.

Conflicts of interest

There are no conflicts to declare.

Acknowledgements

The Authors are grateful for the grant support of University of Tabriz.

References

1 S. M. S. Murshed, *Advanced Cooling Technologies and Applications*, BoD – Books on Demand, 2019.
2 A. Ghadimi, R. Saidur and H. S. C. Metselaar, *Int. J. Heat Mass Transfer*, 2011, **54**, 4051–4068.

© 2024 The Author(s). Published by the Royal Society of Chemistry

Open Access Article. Published on 22 October 2024. Downloaded on 5/3/2026 10:35:04 AM. This article is licensed under a Creative Commons Attribution-NonCommercial 3.0 Unported Licence.

3 J. E. Yumi, T. J. Moreno and G. C. Chango, *Lat. Am. Appl. Res.*, 2023, **53**, 77–88.
4 K. A. Jehhef and M. Siba, *Acta Mech. Malaysia*, 2019, **2**, 1–19.
5 S. N. M. Zainon and W. H. Azmi, *Micromachines*, 2021, **12**, 176.
6 J. Wang, X. Yang, J. J. Klemeš, K. Tian, T. Ma and B. Sunden, *Renewable Sustainable Energy Rev.*, 2023, **188**, 113854.
7 J. Silva-Yumi, T. M. Romero and G. C. Lescano, *ESPOCH Congresses: The Ecuadorian Journal of STEAM*, 2021, 998–1006.
8 S. Chakraborty and P. K. Panigrahi, *Appl. Therm. Eng.*, 2020, **174**, 115259.
9 J. Xu and B. Yang, *Nanotechnol. Rev.*, 2013, **2**, 289–306.
10 L. Dan, K. Zhang, Q. Wang and N. Liu, *J. Ind. Eng. Chem.*, 2024, **132**, 518–528.
11 M. Teodorescu and M. Bercea, *Polym.-Plast. Technol. Eng.*, 2015, **54**, 923–943.
12 X. Zhi, H. Fang, C. Bao, G. Shen, J. Zhang, K. Wang, S. Guo, T. Wan and D. Cui, *Biomaterials*, 2013, **34**, 5254–5261.
13 M. M. Fiume, W. F. Bergfeld, D. V Belsito, R. A. Hill, C. D. Klaassen, D. Liebler, J. G. Marks Jr, R. C. Shank, T. J. Slaga and P. W. Snyder, *Int. J. Toxicol.*, 2012, **31**, 245S–260S.
14 M. T. Zafarani-Moattar, H. Shekaari, R. Munes-Rast and R. Majdan-Cegincara, *Fluid Phase Equilib.*, 2015, **403**, 136–144.
15 A. V Lebedev and S. N. Lysenko, *Solid State Phenom.*, 2012, **190**, 649–652.
16 B. Bai, L. Li, Y. Liu, H. Liu, Z. Wang and C. You, *SPE Reservoir Eval. Eng.*, 2007, **10**, 415–422.
17 A. A. Mohammed, H. I. Dawood and H. N. Onyeaka, *IOP Conference Series: Earth and Environmental Science*, IOP Publishing, 2023, vol. 1232, p. 12009.
18 H. Sui, L. Zhang, W. Zong, F. Zhang, R. Liu, C. Gao and C. Li, *J. Dispersion Sci. Technol.*, 2007, **28**, 1316–1324.
19 R. Mueller, R. Jossen, S. E. Pratsinis, M. Watson and M. K. Akhtar, *J. Am. Ceram. Soc.*, 2004, **87**, 197–202.
20 D. G. Syarif, *Adv. Mater. Res.*, 2014, **896**, 163–167.
21 S. U. S. Choi, Z. G. Zhang, Wl. Yu, F. E. Lockwood and E. A. Grulke, *Appl. Phys. Lett.*, 2001, **79**, 2252–2254.
22 M. A. Khairul, K. Shah, E. Doroodchi, R. Azizian and B. Moghtaderi, *Int. J. Heat Mass Transfer*, 2016, **98**, 778–787.
23 N. K. Gupta, S. Mishra, A. K. Tiwari and S. K. Ghosh, *Mater. Today: Proc.*, 2019, **18**, 968–978.
24 K. H. Solangi, S. N. Kazi, M. R. Luhur, A. Badarudin, A. Amiri, R. Sadri, M. N. M. Zubir, S. Gharehkhani and andK. H. Teng, *Energy*, 2015, **89**, 1065–1086.
25 S. J. Thrush, A. S. Comfort, J. S. Dusenbury, Y. Xiong, H. Qu, X. Han, J. D. Schall, G. C. Barber and X. Wang, *Tribol. Trans.*, 2020, **63**, 68–76.
26 Z. Said, L. S. Sundar, A. K. Tiwari, H. M. Ali, M. Sheikholeslami, E. Bellos and H. Babar, *Phys. Rep.*, 2022, **946**, 1–94.
27 S. Hussain, M. Salman, J. P. Youngblood, U. Farooq, S. Yasmeen, K. M. Al-Ahmary and M. Ahmed, *J. Mol. Liq.*, 2024, **411**, 125704.
28 U. M. Kakar, Z. Tauanov, S. Azat, N. A. Ahmadi, M. H. Hassand, A. Sarwari, A. W. Monib and P. Niazi, *J. Chem. Stud.*, 2024, **3**, 7–20.
29 P. C. Mishra, S. K. Nayak and S. Mukherjee, *Int. J. Eng. Res. Technol.*, 2013, **2**, 734–745.
30 K. Apmann, R. Fulmer, A. Soto and S. Vafaei, *Materials*, 2021, **14**, 1291.
31 I. Tavman and A. Turgut, *Microfluidics Based Microsystems: Fundamentals and Applications*, Springer, 2010, pp. 139–162.
32 M. T. Zafarani-Moattar and R. Majdan-Cegincara, *J. Chem. Thermodyn.*, 2012, **54**, 55–67.
33 O. Redlich and A. T. Kister, *Ind. Eng. Chem.*, 1948, **40**, 345–348.
34 J. B. Ott, C. E. Stouffer, G. V. Cornett, B. F. Woodfield, R. C. Wirthlin, J. J. Christensen and U. K. Deiters, *J. Chem. Thermodyn.*, 1986, **18**, 1–12.
35 M. Hosseini and S. Ghader, *J. Mol. Liq.*, 2010, **153**, 139–145.
36 M. T. Zafarani-Moattar and R. Majdan-Cegincara, *Ind. Eng. Chem. Res.*, 2011, **50**, 8245–8262.
37 M. Šárpataky, J. Kurimský and M. Rajňák, *Nanomaterials*, 2021, **11**, 2885.
38 F. Ordóñez, F. Chejne, E. Pabón and K. Cacua, *Ceram. Int.*, 2020, **46**, 11970–11977.
39 S. R. Kumar, H. O. Sharma, S. Kumar and D. K. Patel, *Proc. Inst. Mech. Eng., Part E*, 2023, DOI: **10.1177/09544089231190223**.
40 G. K. Sidhu and R. Kumar, *IOP Conference Series: Materials Science and Engineering*, IOP Publishing, 2018, vol. 360, p. 12038.
41 M. T. Zafarani-Moattar, H. Shekaari, R. Munes-Rast and R. Majdan-Cegincara, *Fluid Phase Equilib.*, 2015, **403**, 136–144.
42 W. Yu, H. Xie, L. Chen and Y. Li, *Thermochim. Acta*, 2009, **491**, 92–96.
43 R. Taylor, S. Coulombe, T. Otanicar, P. Phelan, A. Gunawan, W. Lv, G. Rosengarten, R. Prasher and H. Tyagi, *International Conference on Micro/Nanoscale Heat Transfer*, American Society of Mechanical Engineers, 2012, vol. 54778, pp. 219–234.
44 L. Zhang, Y. Ding, M. Povey and D. York, *Prog. Nat. Sci.*, 2008, **18**, 939–944.
45 S. Wu, D. Zhu, X. Li, H. Li and J. Lei, *Thermochim. Acta*, 2009, **483**, 73–77.
46 H. Shekaari and S. S. Mousavi, *Fluid Phase Equilib.*, 2010, **291**, 201–207.
47 H. Shekaari, M. T. Zafarani-Moattar, M. Mokhtarpour and S. Faraji, *J. Mol. Liq.*, 2019, **289**, 111077.
48 M. N. Roy, V. K. Dakua and B. Sinha, *Int. J. Thermophys.*, 2007, **28**, 1275–1284.
49 A. A. Minea, The Annals of "Dunarea de Jos" University of Galati. Fascicle IX, *Metall. Mater. Sci.*, 2016, **39**, 35–47.
50 S. Medhi, S. Chowdhury, A. Kumar, D. K. Gupta, Z. Aswal and J. S. Sangwai, *J. Petrol. Sci. Eng.*, 2020, **187**, 106826.
51 Y. Sun, W. Zhang, J. Li, R. Han and C. Lu, *Molecules*, 2023, **28**, 4331.
52 J. Kim, Y. Tian and J. Wu, *J. Phys. Chem. B*, 2015, **119**, 12108–12116.

© 2024 The Author(s). Published by the Royal Society of Chemistry

Open Access Article. Published on 22 October 2024. Downloaded on 5/3/2026 10:35:04 AM.
This article is licensed under a Creative Commons Attribution-NonCommercial 3.0 Unported Licence.

53 A. Mondal and S. Ram, *J. Am. Ceram. Soc.*, 2004, **87**, 2187–2194.
54 A. J. Kemeakegha, G. A. Cookey and W.-A. L. Izonfuo, *J. Thermodyn.*, 2015, **2015**, 782138.
55 A. Serna, I. G. de la Fuente, J. A. González, J. C. Cobos and C. Casanova, *Fluid Phase Equilib.*, 1995, **110**, 361–367.
56 T. Otsuka and Y. Chujo, *Polym. J.*, 2008, **40**, 1157–1163.
57 J. B. Ott, P. R. Brown, J. D. Moore and A. C. Lewellen, *J. Chem. Thermodyn.*, 1997, **29**, 149–178.
58 D. J. Luning Prak, *J. Chem. Eng. Data*, 2023, **68**, 1053–1066.
59 D. J. Luning Prak, *J. Chem. Eng. Data*, 2024, **69**, 973–986.
60 M. Mokhtarpour, S. Homayoon-far, H. Shekaari and M. T. Zafarani-Moattar, *J. Chem. Eng. Data*, 2020, **65**, 5369–5383.
61 M. T. Zafarani-Moattar and R. Majdan-Cegincara, *Ind. Eng. Chem. Res.*, 2011, **50**, 8245–8262.
62 M. T. Zafarani-Moattar and R. Majdan-Cegincara, *J. Chem. Thermodyn.*, 2012, **54**, 55–67.
63 M. T. Zafarani-Moattar and R. Majdan-Cegincara, *Fluid Phase Equilib.*, 2013, **354**, 102–108.
64 M. E. Mackay, T. T. Dao, A. Tuteja, D. L. Ho, B. Van Horn, H.-C. Kim and C. J. Hawker, *Nat. Mater.*, 2003, **2**, 762–766.
65 J. Ouyang, B. Han, G. Chen, L. Zhao and J. Ou, *Constr. Build. Mater.*, 2018, **185**, 293–301.
66 H. Saigo, D. B. Kc and N. Saito, *Sci. Rep.*, 2022, **12**, 6541.
67 F. J. Valdes-Parada, J. A. Ochoa-Tapia and J. Alvarez-Ramirez, *Phys. A*, 2007, **385**, 69–79.
68 D. I. Pullin and P. G. Saffman, *Phys. Fluids A*, 1993, **5**, 126–145.
69 Z. An, Y. Zhang, Q. Li, H. Wang, Z. Guo and J. Zhu, *Powder Technol.*, 2018, **328**, 199–206.

© 2024 The Author(s). Published by the Royal Society of Chemistry